ISSN: 2414-1895 DOI: 10.6919/ICJE.202509_11(9).0007

Impact of Temperature Cracks on the Toughness and Load-Bearing Performance of Structural Components

Yue Gao[1,2], Danxiang Ma[1,2,*]

[1] College of Civil and Architectural Engineering, North China Universityof Science and Technology, Tangshan, Hebei 063210, China

[2] Hebei Province Earthquake Engineering Research Center, Tangshan, Hebei 063210, China

[*]E-mail addresses of corresponding author: heiseyouhuo@126.com

Abstract

A simulation of the shear performance of four simply supported beams with existing thermal cracks was conducted. The study investigated the influence of different crack locations and different load positions on the stress intensity factor of the existing thermal cracks. The results indicate that thermal cracks in the midspan of the beam are more likely to propagate new cracks. The smaller the load-to-shear span ratio, the higher the likelihood of the existing thermal cracks continuing to expand. For thermal cracks in the midspan, the possibility of developing into Mode II cracks (shear mode) is relatively high.

Keywords

Thermal Cracks; Finite Element Analysis; Stress Intensity Factor.

1. Introduction

In line with current building codes, structural collapse in the immediate aftermath of a fire is highly unlikely. However, the load-bearing capacity of the structure is inevitably diminished, necessitating an assessment and reinforcement prior to the building's reuse. Following a fire in reinforced concrete structures, the concrete material, which contains inherent moisture, is prone to surface spalling and the development of densely packed crazing cracks. Under subsequent loading conditions, the load-induced cracks on the structural surface typically extend along these pre-existing crazing cracks. Consequently, the presence of crazing cracks substantially affects the progression of crack development in structural members during subsequent stages.

According to the United Nations' terminology, resilience is generally defined as the ability of systems, communities, or societies to resist, absorb, accommodate, adapt to, transform, and recover from the impacts of disasters in a timely and effective manner [1], including the protection and restoration of their critical infrastructure and functions through risk management. The concept of resilience has been evolving over recent years. Manes [2] conducted a comprehensive review of the definitions of resilience found in existing literature: the term resilience in the Presidential Policy Directive of the United States implies the capability to "prepare for and adapt to changing conditions, withstand and rapidly recover from disruptions"; the National Research Council defines resilience as the ability to prepare for, plan, absorb, recover from, or more successfully adapt to actual or potential adverse events. Bruneau [3] developed a conceptual framework for earthquake resilience, which provides a reference for the study of the concept of resilience. This framework illustrates the functional performance of communities under the disruption of disaster events.

Multiple approaches exist for assessing the post-fire resilience of structural members; the most direct is quantifying residual load-bearing capacity through a rigorous computational framework. Such

ISSN: 2414-1895 DOI: 10.6919/ICJE.202509_11(9).0007

assessments are conventionally anchored in fire tests. Kodur [4] proposed a three-stage evaluation method for the residual capacity of post-fire reinforced concrete (RC) beams: (i) structural response under ambient conditions, (ii) thermo-mechanical response during fire exposure, and (iii) residual thermal response after cooling. Finite-element analyses calibrated against test data yield residual capacities that are markedly closer to measured values than those obtained from simplified sectional analyses.

Complementing this framework, Ellingwood [5] identified, via experimental campaigns, the key parameters governing the elevated-temperature capacity of RC beams, notably the degradation of steel strength and the onset of thermal creep. Piet [6] conducted full-scale fire tests on concrete beams under sustained load and derived a mathematical model capable of predicting their fire response. Fan [7] examined the fire performance of two RC beams strengthened with carbon-fiber sheets (CFS) under the ISO 834 standard fire; the findings highlight the shear-span ratio as the dominant factor influencing both fire resistance and failure mode. Choi [8] investigated the influence of concrete compressive strength on the fire performance of RC beams. The results reveal that, except for the uppermost section, the temperature–time histories across the beam depth are virtually identical and independent of concrete strength.

Extensive fire-test data on reinforced-concrete (RC) beams are routinely employed to evaluate residual capacity; however, resilience is of far greater concern in structural engineering. Under fire exposure, RC members rarely reach global collapse but instead develop thermal cracks (Fig. 1). Quantifying the effect of these cracks on structural resilience is therefore paramount, as their presence governs post-fire recovery and serviceability. Figure 2 illustrates how pre-existing thermal cracks dictate subsequent crack propagation under reloading.

Figure 1. Temperature cracks

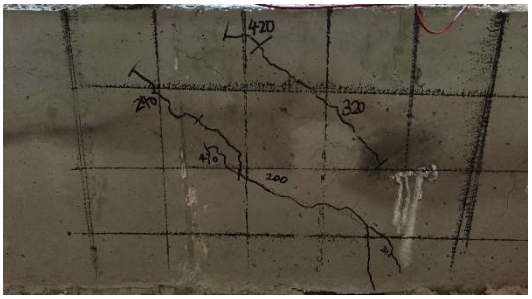

Figure 2. Load-Induced cracks based on temperature crack propagation

This study aims to rigorously quantify how thermal cracks affect the resilience and load-bearing performance of structural members. Using high-fidelity numerical simulations, the roles of shear-span ratio, crack location, and crack length in the evolution of thermal cracks-and their subsequent impact on structural response-are systematically examined. The results will provide a scientific basis for post-fire resilience assessments of building structures.

2. Specimen

To investigate the influence of existing thermal cracks on crack propagation under subsequent loading, a two-dimensional simply supported beam structure was established using the ABAQUS finite element analysis software. The beam was modeled as a linear elastic material with an elastic modulus E=30GPa and a Poisson's ratio v=0.20. The actual dimensions of the beam were 1300mm×200mm×100mm, with a span length of 1000mm and a height of 200mm. The loading was applied using displacement control, with the ultimate deflection set to w=30/l=33mm (where l is the span length). A uniform stepwise loading mechanism was employed, with a total analysis duration of 1s, and a load increment of 3.3mm per step, with each step lasting 0.1s.

ISSN: 2414-1895 DOI: 10.6919/ICJE.202509_11(9).0007

3. Crack Configuration

The finite element analysis considered two primary factors: the location of the thermal cracks and the load-to-shear span ratio. The locations of the thermal cracks included the bottom and the midspan of the beam. Based on previous shear beam test results, cracks in the midspan generally occur along the line connecting the support and the loading point.

Beam L1: The thermal crack is located at the bottom of the beam, oriented vertically. It is situated 150 mm from the support and has a length of 25 mm. The crack is symmetrically arranged on both sides of the beam section. The load-to-shear span ratio is 1.0. The specific configuration is shown in Figure 3.

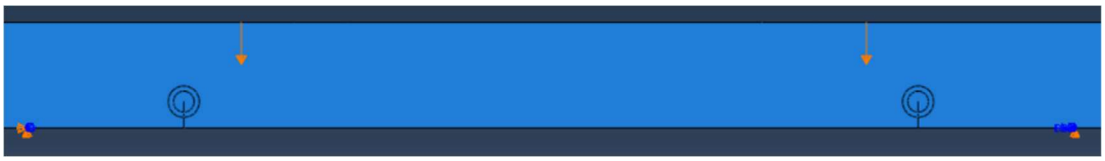

Figure 3. Load arrangement for cracks in beam L1

Beam L2: The thermal crack is located at the bottom of the beam, oriented vertically. It is situated 150 mm from the support and has a length of 25 mm. The crack is symmetrically arranged on both sides of the beam section. The load-to-shear span ratio is 2.0. The specific configuration is shown in Figure 4.

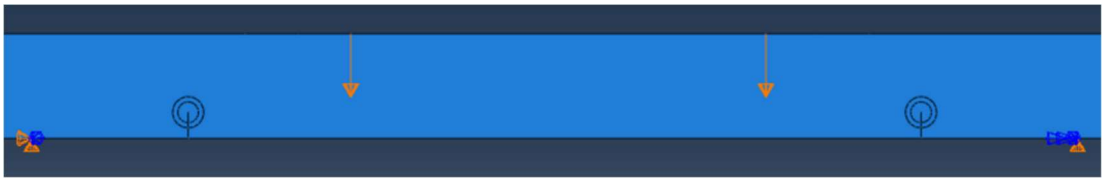

Figure 4. Load arrangement for cracks in beam L2

Beam L3: The thermal crack is located in the midspan of the beam, oriented along the line connecting the support and the loading point. The bottom of the crack is 250 mm horizontally from the support, and the top of the crack is 50 mm vertically from the top of the beam. The total length of the crack is 50 mm. The crack is symmetrically arranged on both the left and right sides of the beam. The load-to-shear span ratio is 1.0. The specific configuration is shown in Figure 5.

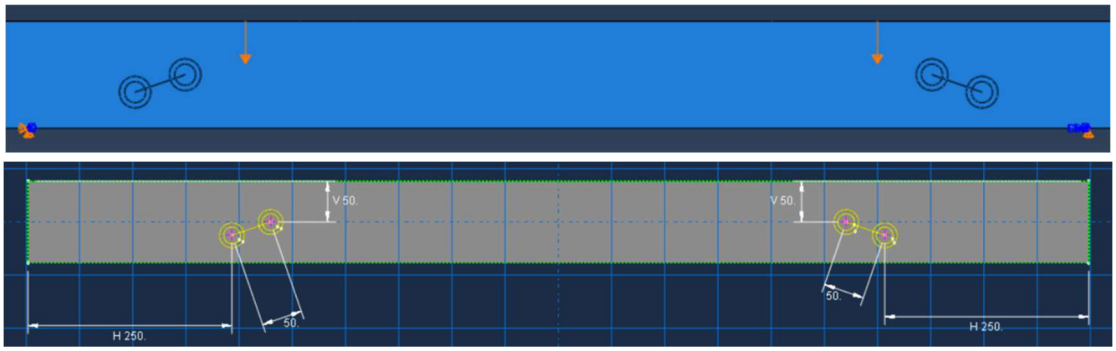

Figure 5. Load arrangement for cracks in beam L3

Beam L4: The thermal crack is located in the midspan of the beam, oriented along the line connecting the support and the loading point. The bottom of the crack is 250 mm horizontally from the support,

ISSN: 2414-1895 DOI: 10.6919/ICJE.202509_11(9).0007

and the top of the crack is 50 mm vertically from the top of the beam. The total length of the crack is 50 mm. The crack is symmetrically arranged on both the left and right sides of the beam. The load-to-shear span ratio is 2.0. The specific configuration is shown in Figure 6.

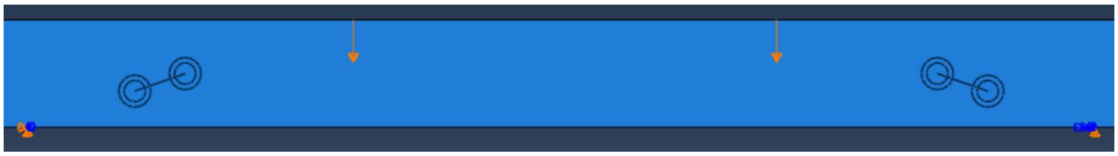

Figure 6. Load arrangement for cracks in beam L4

Table 1. Specimen numbers

Beam	L1	L2	L3	L4
Shear span ratio	1.0	2.0	1.0	2.0
Crack location	Bottom	Bottom	Middle	Middle
Crack length	25	25	50	50

4. Definition of Assigned Joints and Cracks

The straight lines drawn are assigned as joints, as shown in the figure below:

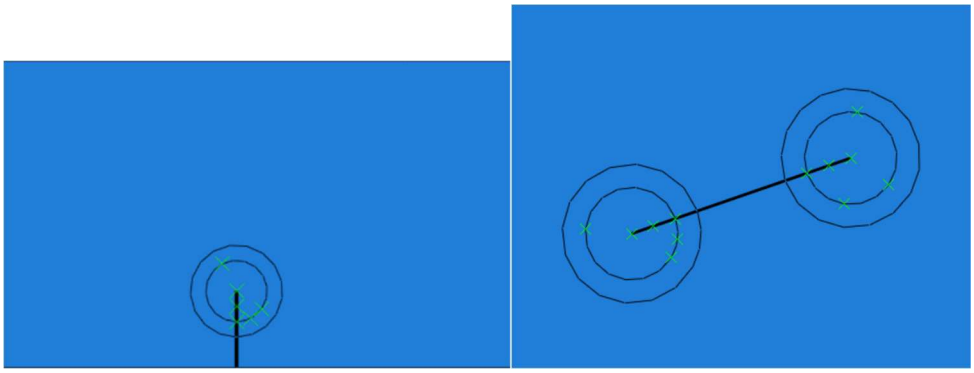

Figure 7. Assignment of joints

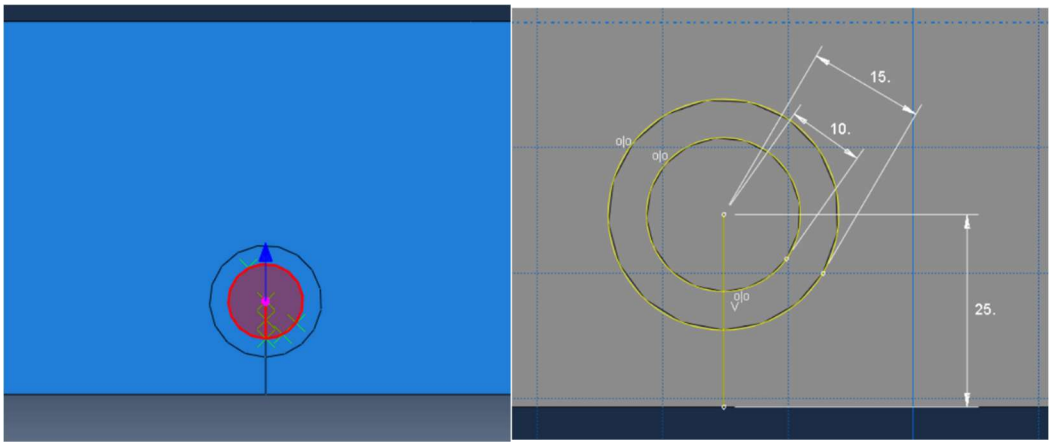

Figure 8. Definition of bottom cracks

The crack type is defined using the contour integral method. To facilitate mesh generation at the crack tip, circles with radii of 10 mm and 15 mm are drawn with the crack tip as the center. The region inside the 10 mm circle is defined as the crack front area. The direction of crack propagation is defined using the vector *q*. Additionally, element singularity is set, with the middle node parameter taken as 0.25. The crack tip degeneration element control is set as: failed element edges, repeated nodes. For

ISSN: 2414-1895 DOI: 10.6919/ICJE.202509_11(9).0007

mid-span cracks, the cracks are defined to extend upwards and downwards, meaning that each crack has two crack tips and two vectors q.

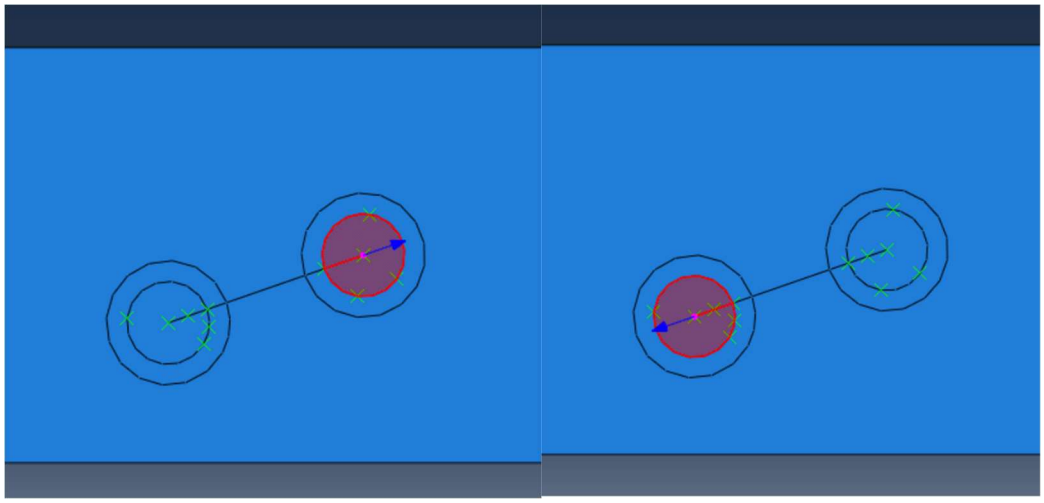

Figure 9. Definition of midspan cracks

5. Mesh Control

The region inside the 10 mm circle at the crack front is set as triangular quadratic elements (CPS6), while the remaining parts are set as quadrilateral quadratic elements (CPS8). The seed size for the mesh around the cracks and circular regions is set to 1 mm, while the seed size for other locations is set to 5 mm. After simulation, it was found that triangular meshes should not appear in the contour integral region, as this meshing method is not suitable for stress intensity factor calculation. Subsequently, for L1, a quadrilateral advanced algorithm mesh and a neutral axis algorithm mesh were used, and the differences between the two were compared. The meshing results are shown in the figure below.

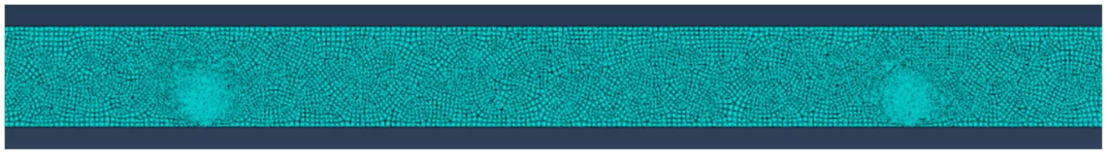

a. Overall mesh division

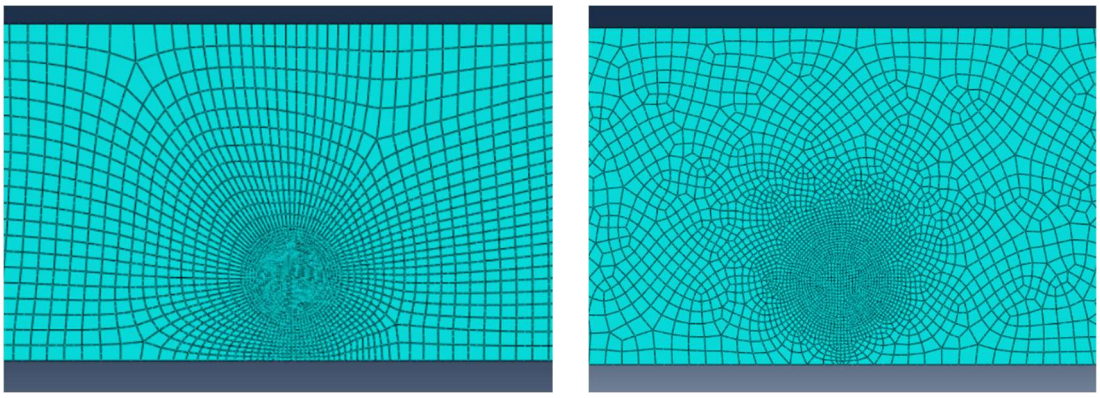

b. Neutral axis algorithm quadrilateral mesh division

c. Advanced algorithm quadrilateral mesh division

Figure 10. Overall mesh and mesh arrangement near cracks

ISSN: 2414-1895 DOI: 10.6919/ICJE.202509_11(9).0007

6. Finite Element Analysis Results

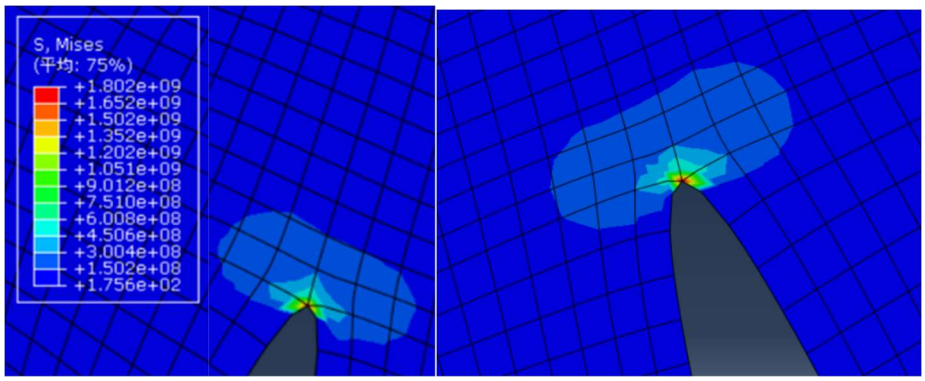

a. Results using neutral axis algorithm quadrilateral mesh

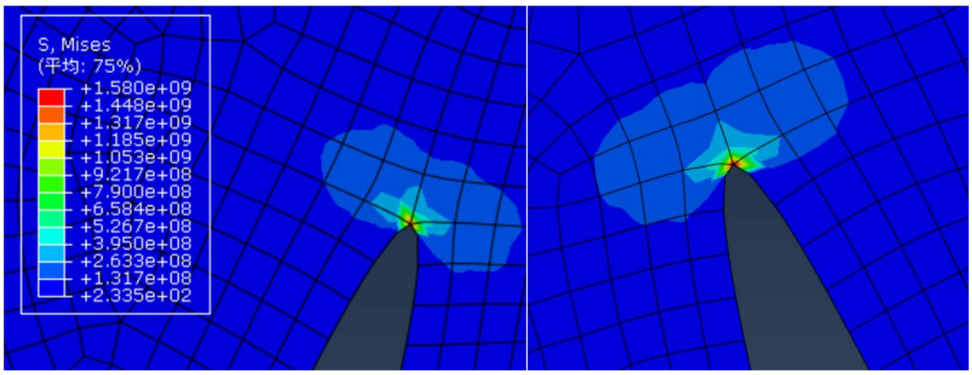

b. Results using advanced algorithm quadrilateral mesh

Figure 11. Comparison of stress contours for different meshing methods of L1

H-OUTPUT-1_CRACK-1				
-22-	K1:	4.2591E+08	4.2591E+08	4.2591E+08
4.2591E+08				
	K2:	3.7112E+07	3.7112E+07	3.7112E+07
3.7112E+07				
H-OUTPUT-2_CRACK-2				
-26-	K1:	4.5531E+08	4.5531E+08	4.5531E+08
4.5531E+08				
	K2:	-3.9209E+07	-3.9209E+07	-3.9209E+07
-3.9209E+07				

a. Stress intensity factor calculation results using neutral axis algorithm quadrilateral mesh

H-OUTPUT-1_CRACK-1				
-22-	K1:	4.2490E+08	4.2490E+08	4.2490E+08
4.2490E+08				
	K2:	3.7017E+07	3.7017E+07	3.7017E+07
3.7017E+07				
H-OUTPUT-2_CRACK-2				
-26-	K1:	4.5671E+08	4.5671E+08	4.5671E+08
4.5671E+08				
	K2:	-3.9333E+07	-3.9333E+07	-3.9333E+07
-3.9333E+07				

b.Stress intensity factor calculation results using advanced algorithm quadrilateral mesh

Figure 12. Comparison of stress intensity factors for different meshing methods of L1

ISSN: 2414-1895 DOI: 10.6919/ICJE.202509_11(9).0007

Two different meshing methods were applied to L1, and the resulting stress contour diagrams are shown in Figure 11 below. It can be observed that there is a certain difference in the stress values at the crack tips. The maximum stress value at the crack tip using the neutral axis algorithm mesh is 1802 MPa, while that using the advanced algorithm mesh is 1580 MPa. There is a noticeable difference between the two. Based on the mesh quality, the remaining specimens were meshed using the advanced algorithm.

As shown in the figure above, for Crack 1, the stress intensity factor using the neutral axis algorithm for the quadrilateral mesh is K1=425.9$MPa\sqrt{mm}$, while using the advanced algorithm for the quadrilateral mesh, the stress intensity factor is K1=456.7$MPa\sqrt{mm}$. For the Mode II stress intensity factor, the neutral axis algorithm yields K2=371.1$MPa\sqrt{mm}$, and the advanced algorithm yields K2=370.1$MPa\sqrt{mm}$.For Crack 2, the stress intensity factor using the neutral axis algorithm for the quadrilateral mesh is K1=455.3$MPa\sqrt{mm}$, while using the advanced algorithm for the quadrilateral mesh, the stress intensity factor is K1=424.9$MPa\sqrt{mm}$. For the Mode II stress intensity factor, the neutral axis algorithm yields K2=392.1 $MPa\sqrt{mm}$, and the advanced algorithm yields K2=393.3$MPa\sqrt{mm}$.

It is evident that the stress intensity factors vary depending on the meshing method used. As for the comparison of the advantages and disadvantages between the two methods, further corresponding experiments are required to make a judgment.

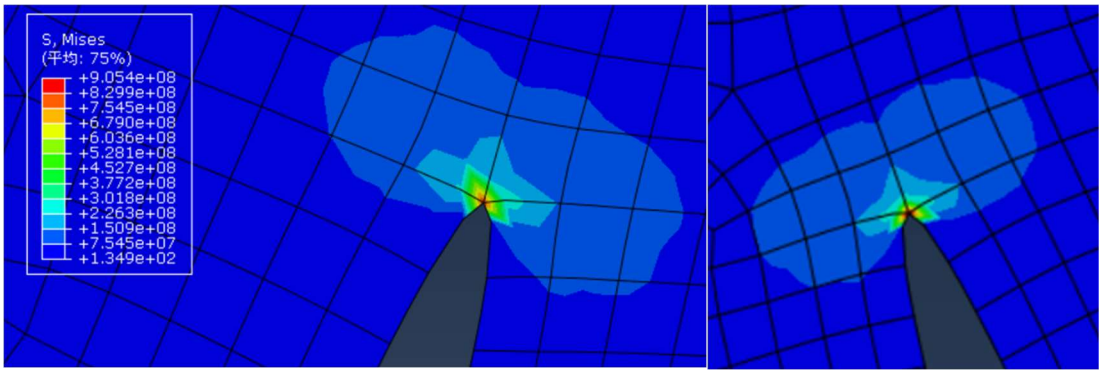

Figure 13. Stress contours at crack tips for L2

H-OUTPUT-1_CRACK-1				
-21-	K1:	2.4510E+08	2.4510E+08	2.4510E+08
	K2:	2.1004E+07	2.1004E+07	2.1004E+07
H-OUTPUT-2_CRACK-2				
-25-	K1:	2.6171E+08	2.6171E+08	2.6171E+08
	K2:	-2.2447E+07	-2.2447E+07	-2.2447E+07

Figure 14. Calculation results of stress intensity factors for L2

For Crack 1, the stress intensity factor (K1) calculated using the advanced algorithm for the quadrilateral mesh is 245.1$MPa\sqrt{mm}$, and the stress intensity factor (K2) is 210 $MPa\sqrt{mm}$. For Crack 2, the stress intensity factor (K1) calculated using the advanced algorithm for the quadrilateral mesh is 261.7 $MPa\sqrt{mm}$, and the stress intensity factor (K2) is 224.4 $MPa\sqrt{mm}$. The comparison between L1 and L2 is shown in Table 2 below.

ISSN: 2414-1895 DOI: 10.6919/ICJE.202509_11(9).0007

Table 2. Comparison of stress intensity factors between L1 and L2

Beam	L1		L2	
	Crack1	Crack2	Crack1	Crack2
K1	456.7	424.9	245.1	261.7
K2	370.1	393.3	210	224.4

As can be seen from the comparison, when the crack locations are the same, the stress intensity factors differ significantly between beams with different shear span ratios. Taking the stress intensity factor (K1) of Crack 1 as an example, the ratio of the stress intensity factor (K2) of Beam L1 to that of Beam L2 is $K1_{L1}/ K1_{L2}$=456.7/245.1=1.86. This indicates that the load position has a significant impact on the stress intensity factor of beam cracks. For future research, specific material constitutive relationships can be set to more accurately reflect the influence of load position, providing a basis for the study of crack propagation in reinforced concrete beams.

As shown in Figure 15, the stress contour diagrams for mid-span cracks with a shear span ratio of 1.0 are presented. In Figure a (left side) and Figure b (right side), the crack tip at the bottom is depicted. It can be observed from the stress contour diagrams that the stress values at the crack tip at the bottom are significantly higher than those at the crack tip at the top. This observation, combined with the stress intensity factors, can be used for further in-depth analysis.

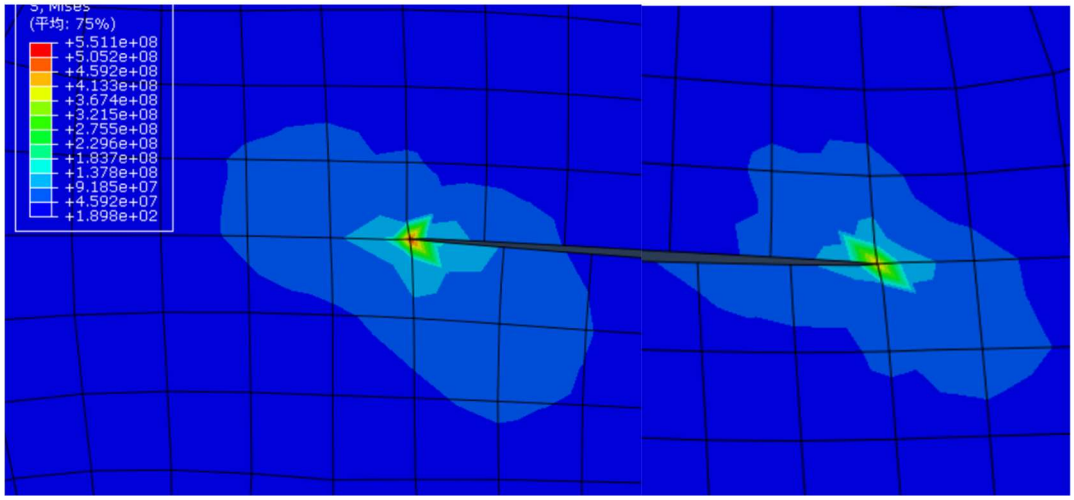

a. Left crack

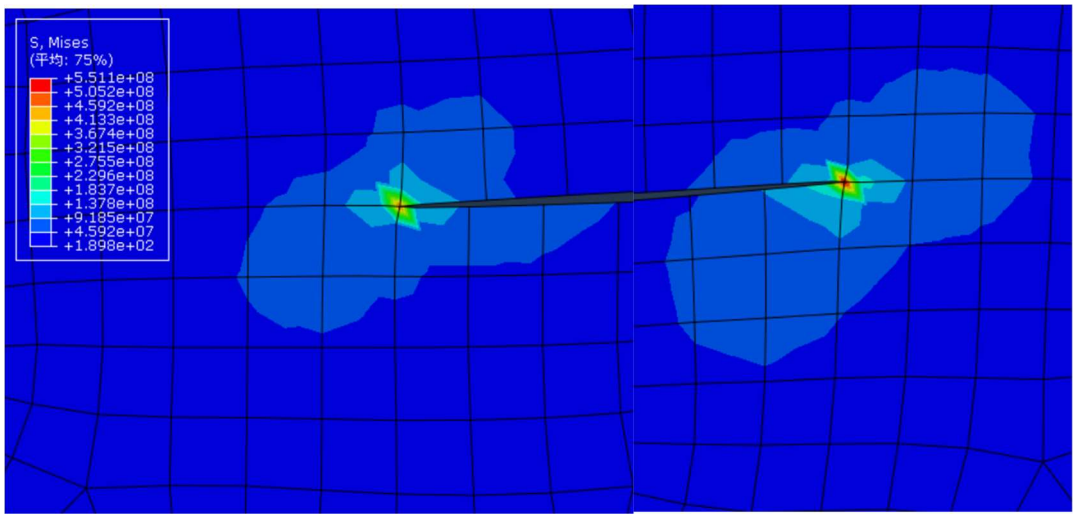

b. Right crack

Figure 15. Stress contours at crack tips of L3

ISSN: 2414-1895 DOI: 10.6919/ICJE.202509_11(9).0007

H-OUTPUT-1_CRACK-1
-20- K1: 6.0712E+07 6.0712E+07 6.0712E+
07 6.0712E+07 6.0712E+07
K2: -7.0382E+07 -7.0382E+07 -7.0382E+
07 -7.0382E+07 -7.0382E+07

H-OUTPUT-2_CRACK-2
-24- K1: 6.1367E+07 6.1367E+07 6.1367E+
07 6.1367E+07 6.1367E+07
K2: -8.4886E+07 -8.4886E+07 -8.4886E+
07 -8.4886E+07 -8.4886E+07

H-OUTPUT-3_CRACK-3
-28- K1: 6.4747E+07 6.4747E+07 6.4747E+
07 6.4747E+07 6.4747E+07
K2: 7.6603E+07 7.6603E+07 7.6603E+
07 7.6603E+07 7.6603E+07

H-OUTPUT-4_CRACK-4
-32- K1: 6.6399E+07 6.6399E+07 6.6399E+
07 6.6399E+07 6.6399E+07
K2: 9.2049E+07 9.2049E+07 9.2049E+
07 9.2049E+07 9.2049E+07

Figure 16. Calculation results of stress intensity factors for L3

For specimen L3, the stress intensity factors are summarized in Table 3 below. It can be seen that for the two cracks along the same joint (Crack 1, which propagates upwards, and Crack 2, which propagates downwards), the Mode I stress intensity factors (K1) are similar in value. However, the Mode II stress intensity factors (K2) differ significantly, with a difference of 145 $MPa\sqrt{mm}$. This indicates that the crack propagation tendency is more inclined to develop downwards.

Table 3. Stress intensity factors for L3

Beam	Crack1	Crack2	Crack3	Crack4
K1	607.1	613.6	647.4	663.9
K2	703.8	848.8	766.0	920.4

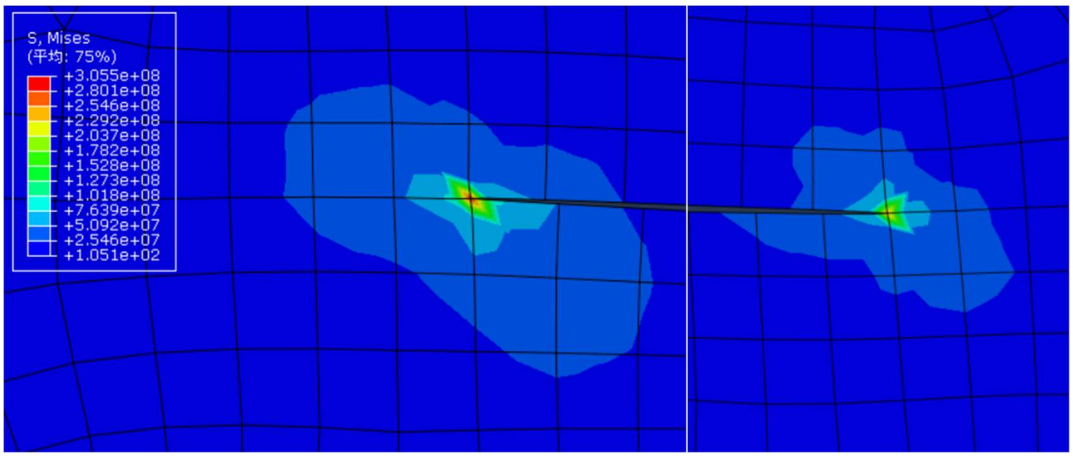

a. Left crack

ISSN: 2414-1895 DOI: 10.6919/ICJE.202509_11(9).0007

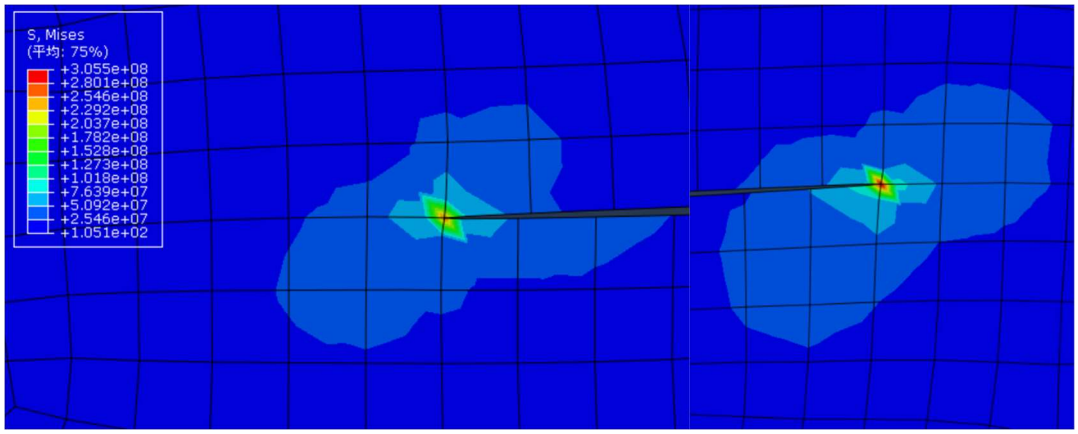

b. Right crack

Figure 17. Advanced mesh control results for L4

H-OUTPUT-1_CRACK-1

-18-	K1:	3.4219E+07	3.4219E+07	3.4219E+07
		3.4219E+07	3.4219E+07	
	K2:	-3.9723E+07	-3.9723E+07	-3.9723E+07
		-3.9723E+07	-3.9723E+07	

H-OUTPUT-2_CRACK-2

-22-	K1:	3.3902E+07	3.3902E+07	3.3902E+07
		3.3902E+07	3.3902E+07	
	K2:	-4.7767E+07	-4.7767E+07	-4.7767E+07
		-4.7767E+07	-4.7767E+07	

H-OUTPUT-3_CRACK-3

-26-	K1:	3.6661E+07	3.6661E+07	3.6661E+07
		3.6661E+07	3.6661E+07	
	K2:	4.2525E+07	4.2525E+07	4.2525E+07
		4.2525E+07	4.2525E+07	

H-OUTPUT-4_CRACK-4

-30-	K1:	3.6310E+07	3.6310E+07	3.6310E+07
		3.6310E+07	3.6310E+07	
	K2:	5.1151E+07	5.1151E+07	5.1151E+07
		5.1151E+07	5.1151E+07	

Figure 18. Calculation results of stress intensity factors for L4

For specimen L4, the stress intensity factors are summarized in Table 4 below. It can be seen that, similar to L3, the Mode I stress intensity factors (K1) for cracks along the same joint are close in value, while the Mode II stress intensity factors (K2) differ significantly. For example, the difference is 80.4 $MPa\sqrt{mm}$. This indicates that, for midspan cracks with different shear span ratios, the crack propagation tendency is also more inclined to develop downwards.

When comparing specimens L3 and L4, it is evident that the stress intensity factors for the same crack locations in L3 are much higher than those in L4. Taking (K1) of Crack 1 as an example, the ratio of the stress intensity factor (K1) of Beam L3 to that of Beam L4 is $K1_{L3}$/ $K1_{L4}$=607.1/342.2=1.77. This shows that the shear span ratio has a significant impact on the stress intensity factors of beam cracks.

ISSN: 2414-1895 DOI: 10.6919/ICJE.202509_11(9).0007

Table 4. Stress intensity factors for L4

Beam	Crack1	Crack2	Crack3	Crack4
K1	342.2	339.0	366.6	363.1
K2	397.2	477.6	425.2	511.5

Table 5. Comparison of stress intensity factors for different crack locations

Beam	Crack	K1	K2
L1	Crack1	456.7	370.1
	Crack2	424.9	393.3
L2	Crack1	245.1	210
	Crack2	261.7	224.4
L3	Crack1	607.1	703.8
	Crack2	613.6	848.8
	Crack3	647.4	766.0
	Crack4	663.9	920.4
L4	Crack1	342.2	397.2
	Crack2	339.0	477.6
	Crack3	366.6	425.2
	Crack4	363.1	511.5

Comparison of Specimens L1 and L3,with the same load shear span ratio, the overall stress intensity factors of Specimen L3 are much higher than those of Specimen L1. For example, for the upward-propagating Crack 1, the ratio of the stress intensity factor (K1) of Beam L3 to that of Beam L1 is $K1_{L3}$/ $K1_{L1}$=607.1/456.7=1.33. This indicates that different crack locations have a significant impact on the crack propagation and the load-bearing capacity of the beam under normal temperature conditions.

7. Conclusion

(1) Mesh Control Methods: Different mesh control methods result in different stress intensity factors and crack tip stress values. Experimental validation is necessary to correct these differences.

(2) Load Position and Shear Span Ratio: The location of the load significantly affects the stress intensity factors of beam cracks. A smaller shear span ratio (i.e., closer load position to the crack) results in higher stress intensity factors, bringing the crack closer to the cracking state.

(3) Crack Propagation Direction in Midspan Cracks: For midspan cracks, the Mode I stress intensity factors (K1) for upward-propagating and downward-propagating cracks are similar. However, the Mode II stress intensity factors (K2) differ significantly, with a greater tendency for downward-propagating II-type cracks.

(4) Influence of Crack Location: Crack location has a significant impact on the crack propagation and load-bearing capacity of the beam. Midspan cracks are more likely to develop into loading cracks compared to bottom cracks, affecting the beam's performance under subsequent loading and normal temperature conditions.

References

[1] UNISDR. 2009 UNISDR terminology on disaster risk reduction [EB/OL.]. https://www.undrr.org/publication/2009-unisdr-terminology-disaster-risk-reduction, 2009-01-23.

[2] Manes M. Towards resilience evaluation of buildings when exposed to fire based on English and USA fire statistics[D]. University of Edinburgh, 2021.

[3] Bruneau M, Chang S E, Eguchi R T, et al. A framework to quantitatively assess and enhance the seismic resilience of communities[J]. Earthquake Spectra, 2003, 19(4): 733-752.

ISSN: 2414-1895 DOI: 10.6919/ICJE.202509_11(9).0007

[4] Kodur V K R, Agrawal A. An approach for evaluating residual capacity of reinforced concrete beams exposed to fire[J]. Engineering Structures, 2016,110:293-306.DOI:https://doi.org/10.1016/j.engstruct.2015.11.047.

[5] Ellingwood B R, Shaver J R. Reliability of RC Beams Subjected to Fire[J]. Journal of the Structural Division, 1977, 103(5):1047-1059.

[6] Lin, T.D., Ellingwood, B. Flexural and shear behavior of reinforced concrete beams during fire tests[J]. Flexural Strength, 1988, 12:81.

[7] Fan H, Fan Z. Studies on fire resistance of FRP shear strengthened reinforced concrete beams[J]. Applied Mechanics and Materials, 2011, 94-96:4. DOI:https://doi.org/10.4028/www.scientific.net/AMM.94-96.1318

[8] Choi E G. The structural behavior and simplified thermal analysis of normal-strength and high-strength concrete beams under fire[J]. Engineering Structures, 2011, 33(4):1123-1132. DOI:https://doi.org/10.1016/j.engstruct.2010.12.030